JACS JOURNAL OF THE AMERICAN CHEMICAL SOCIETY

Article

Cite This: J. Am. Chem. Soc. 2019, 141, 17394−17403

pubs.acs.org/JACS

How [FeFe]-Hydrogenase Facilitates Bidirectional Proton Transfer

Moritz Senger,[†] Viktor Eichmann,[†] Konstantin Laun,[†] Jifu Duan,[‡] Florian Wittkamp,[§] Günther Knör,[∥] Ulf-Peter Apfel,[§,⊥] Thomas Happe,[‡] Martin Winkler,[‡] Joachim Heberle,[†] and Sven Timo Stripp*[,†]

[†]Experimental Molecular Biophysics, Department of Physics, Freie Universität Berlin, Arnimallee 14, 14195 Berlin, Germany

[‡]Photobiotechnology, Faculty of Biology and Biotechnology and [§]Activation of Small Molecules, Faculty of Chemistry and Biochemistry, Ruhr-Universität Bochum, Universitätsstraße 150, 44801 Bochum, Germany

[∥]Institute of Inorganic Chemistry, Johannes Kepler Universität Linz, Altenberger Straße 69, 4040 Linz, Austria

[⊥]Fraunhofer UMSICHT, 46047 Oberhausen, Germany

Supporting Information

ABSTRACT: Hydrogenases are metalloenzymes that catalyze the conversion of protons and molecular hydrogen, H_2. [FeFe]-hydrogenases show particularly high rates of hydrogen turnover and have inspired numerous compounds for biomimetic H_2 production. Two decades of research on the active site cofactor of [FeFe]-hydrogenases have put forward multiple models of the catalytic proceedings. In comparison, our understanding of proton transfer is poor. Previously, residues were identified forming a hydrogen-bonding network between active site cofactor and bulk solvent; however, the exact mechanism of catalytic proton transfer remained inconclusive. Here, we employ *in situ* infrared difference spectroscopy on the [FeFe]-hydrogenase from *Chlamydomonas reinhardtii* evaluating dynamic changes in the hydrogen-bonding network upon photoreduction. While proton transfer appears to be impaired in the oxidized state (**Hox**), the presented data support continuous proton transfer in the reduced state (**Hred**). Our analysis allows for a direct, molecular unique assignment to individual amino acid residues. We found that transient protonation changes of glutamic acid residue E141 and, most notably, arginine R148 facilitate bidirectional proton transfer in [FeFe]-hydrogenases.

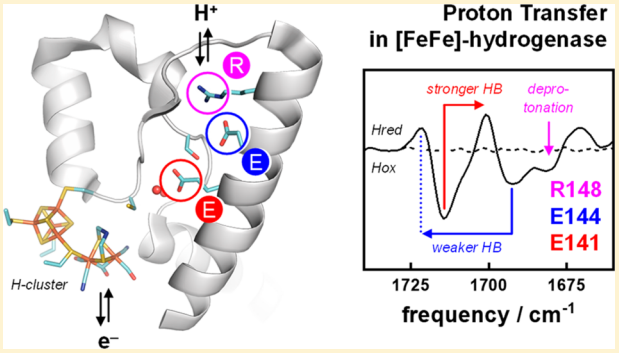

INTRODUCTION

Hydrogenases are gas-processing iron−sulfur enzymes that catalyze the reversible reduction of protons to molecular hydrogen in all kingdoms of life.[1,2] Most hydrogenases are biased toward H_2 oxidation, for example, in the context of energy metabolism and H_2 sensing.[3−5] The [FeFe]-hydrogenases from bacteria and algae, in contrast, are truly bidirectional and catalyze H_2 oxidation and H_2 evolution with similar efficiency.[6−8] Combining high turnover frequencies (10 000 H_2 s^{-1}) and a catalytic midpoint potential close to the H^+/H_2 redox couple,[9−11] the active site cofactor of [FeFe]-hydrogenases ("H-cluster") inspired the design of numerous biomimetic complexes for H_2 production.[12−14]

The H-cluster comprises a conventional [4Fe-4S] center linked to a bimetallic iron−sulfur complex (Figure 1a).[15−17] The diiron site carries two terminal carbonyl and cyanide ligands (CO, CN^-) as well as a single carbonyl ligand in Fe−Fe bridging position (μCO).[18−20] An aminodithiolate (ADT) group connects the proximal and distal iron ion (Fe_p and Fe_d, relative to the [4Fe-4S] center)[21] and functions as proton relay between active site cofactor and protein environment.[22] While prokaryotic [FeFe]-hydrogenases like CPI from *Clostridium pasteurianum* and DDH from *Desulfovibrio desulfuricans* hydrogenase) bind additional iron−sulfur clusters, the enzyme from *Chlamydomonas reinhardtii* (HYDA1) exclusively carries the H-cluster.[6]

During hydrogen turnover, the H-cluster adopts different redox and protonation states. The oxidized resting state (**Hox**)[23−25] can be distinguished from intermediates with a reduced [4Fe-4S] center (**Hred′**, **Hhyd**)[26−32] or a reduced diiron site (**Hred**, **Hsred**).[33−35] These states are formed upon concerted proton and electron transfer. The active-ready geometry of **Hox** is characterized by a square-pyramidal configuration of both metal ions, a μCO ligand, and an open coordination site at Fe_d.[15−17] While this geometry is conserved in **Hred′** and **Hhyd**,[27,30] the structural changes upon reduction of the diiron site are under debate.[36] The H-cluster may undergo rigorous ligand rearrangement forming a μH geometry, which would exclude both **Hred** and **Hsred** from catalytic turnover.[35] Alternatively, diiron site geometries with a bridging[37,38] or "semi-bridging" CO ligand[20] have been

Received: August 26, 2019
Published: October 3, 2019

DOI: 10.1021/jacs.9b09225
J. Am. Chem. Soc. 2019, 141, 17394−17403

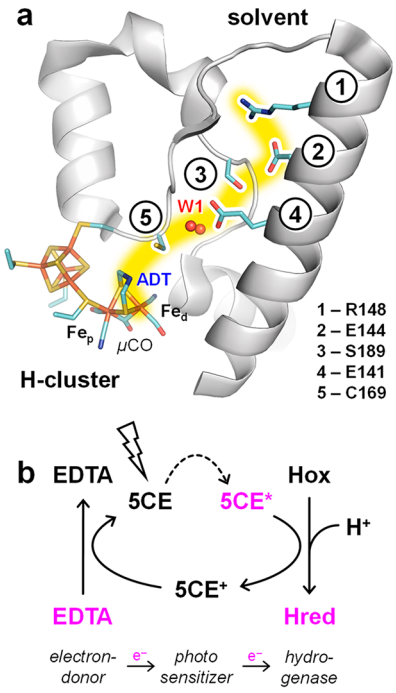

Figure 1. The proton transfer pathway of [FeFe]-hydrogenases and experimental strategy. (a) Hydrogen turnover is catalyzed at the H-cluster that is formed by a diiron site attached to the protein via a [4Fe-4S] center. The diiron site binds five to six CO and CN^- ligands, one of which can be found in Fe−Fe bridging position (μCO). The ADT group functions as proton relay between C169 and the *distal* iron ion of the H-cluster, Fe_d. Residues involved in proton transfer are identified. Cartoon model of the oxidized [FeFe]-hydrogenase from CPI according to pdb entry 4XDC, numbering refers to HYDA1. (b) *Steady-state* illumination of 5′-carboxy eosin Y (5CE, photosensitizer) at 505 nm populated the excited triplet state, 5CE*. The latter was quenched by the oxidized enzyme to enrich **Hred** over **Hox**. Increasing the basicity upon reduction induces a protonation of the H-cluster. The associated changes in the hydrogen-bonding network of the catalytic proton transfer pathway are followed by *in situ* ATR FTIR difference spectroscopy. The sacrificial electron donor EDTA rereduced $5CE^+$ to 5CE.

suggested. On the basis of the assumption of a protonated ADT group in these species, the nomenclature $HredH^+$ and $HsredH^+$ can be found in literature.[34]

[FeFe]-hydrogenases exchange protons with the bulk solvent via a trajectory of conserved, polar amino acid residues that connect active site cofactor and protein surface (Figure 1a).[39−41] Making use of protein crystallography and infrared spectroscopy, previously we were able to identify the residues that render catalytic proton transfer possible.[42] In the [FeFe]-hydrogenase from *C. reinhardtii*, this includes R148, E144, S189, E141, C169 (numbers 1−5 in Figure 1a), and water cluster W1. A second, mostly aqueous proton transfer pathway facilitates protonation of the [4Fe-4S] center.[27] These protons are not consumed in the H_2 release reaction but stabilize the active-ready geometry and compensate for the drop in redox potential after a first reduction step.[26,32] The dynamics of catalytic proton transfer have been addressed by molecular dynamics simulations before;[43−45] however, no experimental data exist on the changes in the hydrogen-bonding network, for example, when switching from H_2 evolution to H_2 oxidation. Such data are key to understanding the bidirectional catalysis of [FeFe]-hydrogenases.

The high extinction coefficient of the active site CO and CN^- ligands facilitated numerous investigations of the H-cluster by Fourier-transform infrared (FTIR) spectroscopy.[25−34] In chromophoric proteins, FTIR difference spectroscopy is routinely used for the analysis of light-induced proton transfer steps.[46−48] However, compared to the H-cluster ligands, the involved amino acid side chains exhibit a drastically lower extinction coefficient and overlap with the intense absorption bands of liquid water and the protein backbone. [FeFe]-hydrogenases lack a natural chromophore to selectively trigger catalytic activity and protonation changes by light, which renders an analysis of proton transfer challenging. Redox dyes provides an opportunity to characterize hydrogen-bonding networks in visibly transparent enzymes.[49]

Here, we explore the dynamics of proton transfer in HYDA1 using *in situ* attenuated total reflection (ATR) FTIR difference spectroscopy. We report *steady-state* photoreduction of the H-cluster in the presence of 5′-carboxy eosin Y (5CE)[50] that resulted in a fast ($t_{1/2} \approx 20$ s), near complete (>90%), and highly selective redox conversion (<5% other species) of the one-electron reduced state **Hred** over the oxidized resting state, **Hox** (Figure 1b). These parameters were not achieved by *in situ* gas treatments[27,30] or electrochemical titrations.[32,35] The proton uptake associated with formation of **Hred** induced spectral differences in the IR regime from 1750 to 1650 cm^{-1}. Exploiting *in situ* H/D exchange and site-directed mutagenesis, these differences are assigned to the C═O stretching vibrations of carboxylic acid side chains (COOH) and the coupled vibrational mode of an protonated arginine side chain ($C(NH_2)_3^+$). Infrared spectroscopy provides evidence for changes in hydrogen bonding involving glutamic acid E141 and serine S189 close to the active site as well as glutamic acid E144 and arginine R148 near the protein surface. This work presents the first direct, experimental characterization of the hydrogen-bonding network that facilitates catalytic proton transfer in [FeFe]-hydrogenases.

EXPERIMENTAL SECTION

The [FeFe]-hydrogenase from *C. reinhardtii* HYDA1 was expressed and synthesized in *Escherichia coli*, purified by strep-tactin affinity chromatography, and activated *in vitro* with synthetic ADT-containing diiron complex under anaerobic conditions.[51,52] After removal of excess complex, the protein concentration was adjusted to ∼3 mM (∼150 g/L). 5′-Carboxy eosin Y (5CE)[50] and ethylenediaminetetraacetic acid (EDTA) were prepared in aqueous stock solutions of 6 and 90 mM, respectively. One part of each component was mixed to yield a HYDA1/5CE/EDTA ratio of 1:2:30.

All spectroscopic experiments were performed under anaerobic conditions, at room temperature, ambient pressure, and on hydrated protein films of physiological pH values. First, 1−2 μL of the reaction mix was pipetted onto the silicon crystal of the ATR unit (DuraDisc SamplIR-2, Smiths Detection) in the FTIR spectrometer (Tensor 27, Bruker). Spectra from 3900−1300 cm^{-1} were recorded with a narrow-band mercury cadmium telluride (MCT) detector with a spectral resolution of 2 cm^{-1} and 25 interferometer scans each (80 kHz). The solution was protected from stray light, dried under N_2, and rehydrated via the gas phase with 10 mM 2-(*N*-morpholino)-ethanesulfonic acid (MES) buffer (pH 6). Traces of reduced and CO-inhibited species were lost in favor of **Hox** upon auto-oxidation.[27]

For the pH jump experiments, guanidine-HCl was solved in H_2O or D_2O. Ten microliters of a 1000 g L^{-1} guanidine-HCl solution (pH ≈∼ 8) was pipetted onto the ATR crystal and continuously measured by FTIR spectroscopy. Addition of 1 μL of NaOH solution (∼100 g L^{-1}, in H_2O or D_2O) increased the bulk pH above the pK_a of guanidine-HCl (∼13.5) deprotonating the guanidinium ion.

DOI: 10.1021/jacs.9b09225
J. Am. Chem. Soc. 2019, 141, 17394−17403

RESULTS

The experiment was initiated upon *steady-state* illumination of the film at 505 nm and followed by FTIR spectroscopy with a time resolution of 5 s (up to 60 s, see Figure S1). After ~20 s, half of the **Hox** population converted into **Hred**. Importantly, no other reduced species than **Hred** were observed, although H_2 released upon reduction of HYDA1[50] may reeact with the enzyme forming **Hred′**, **Hsred**, and **Hhyd**. Therefore, the continuous exchange of gas in our setup was found to be of particular importance, as it precludes reoxidation of H_2 and a buildup of multiple reduced species.[22] No photoreduction was observed under off-resonant conditions (590 nm), whereas illumination at 455 nm induced notable H-cluster corruption (Figure S2), as noted earlier.[53]

Figure 2a shows an overlay of absorbance spectra in the range of 3900−1300 cm^{-1} in the dark (black) and light (magenta). The absorbance ratio of ~1.3 for amide I (1635 cm^{-1}) to amide II (1545 cm^{-1}) suggests a well-hydrated protein film.[27] From 2700 to 1800 cm^{-1} neither liquid water (H_2O) nor protein solution show strong IR intensities, which allows analyzing the CO/CN^- bands of the H-cluster in absolute spectra. The inset highlights the IR signature of the H-cluster from 2150 to 1750 cm^{-1}. The difference spectrum in Figure 2b emphasizes how the hydrogenase adopted **Hox** in the dark while **Hred** clearly dominated upon illumination. The respective IR band patterns have been identified earlier.[34,35] Fitting these patterns to absolute spectra before and after illumination indicated a redox conversion larger than 90%.

In contrast to the CO/CN^- bands, the intense absorbance of liquid water (HOH bending) and protein backbone (amide I, amide II) overlaps with signals in the COOH regime from 1750 to 1650 cm^{-1} and precludes any meaningful analysis in absolute spectra. Figure 2c shows a "dark−light" difference spectrum computed from the single channel spectra that generated the absorbance spectra in Figure 2a. The cofactor bands clearly dominate the spectrum. Efficient photoreduction prevents an accumulation of unspecific changes in the film (i.e., hydration level, protein concentration) and allows analyzing the full spectrum. This includes the OH, SH, and COOH regime as well as frequencies less than 1600 cm^{-1} comprising marker bands of the photosensitizer 5CE (Figure S2).

All difference bands in the COOH regime are specific for functional HYDA1. The inset in Figure 2c shows that no such changes were observed when HYDA1 apoprotein was probed (apo-HYDA1 lacks the diiron site and is catalytically unreactive[51,52]). Moreover, difference spectra of HYDA1 recorded upon exposure to CO (**Hox-CO** over **Hox**) or in the presence of zinc porphyrin as an alternative redox dye[54] (**Hred′** over **Hox**) confirmed that all bands in the COOH regime are specific for the formation of **Hred** (Figure S3).

It is important to point out that our results do not suggest protonation or hydrogen-bonding differences involving OH or SH groups (Figure S4). The former would give rise to sharp absorbance bands around 3650 cm^{-1} indicative of "dangling", weakly hydrogen-bonded water.[55,56] The SH group absorbs around 2550 cm^{-1} and is very sensitive to changes in hydrophilicity.[56−58] Typically, this frequency regime is addressed to analyze hydrogen-bonding changes involving the side chain of a cysteine, for example, C169. Comparing our data with recent work by Hirota et al. on [NiFe]-hydrogenases[58] shows that the signal-to-noise ratio of the **Hred** − **Hox** difference spectrum would allow identifying potential

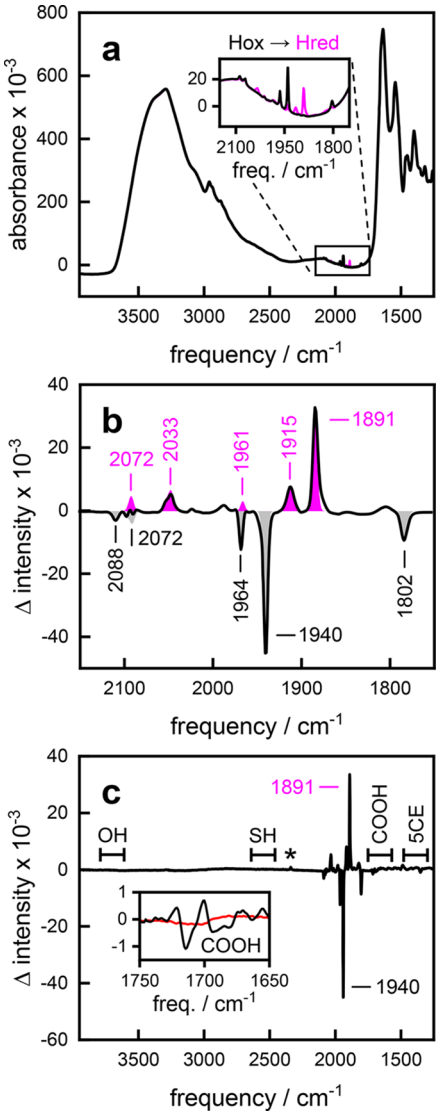

Figure 2. Absorbance and light-induced difference spectra of [FeFe]-hydrogenase. (a) ATR FTIR absorbance spectra of the hydrated reaction mixture (HYDA1/5CE/EDTA) in the dark (black) and upon illumination at 505 nm (magenta). (inset) Magnification of the cofactor regime (2150−1750 cm^{-1}). (b) Subtraction of single channel spectra from the same data set. The dark−light difference spectrum in the CO/CN^- regime of the H-cluster shows conversion of **Hox** (black, negative bands) into **Hred** (magenta, positive bands). (c) The full difference spectrum allows analyzing the OH, SH, and COOH regime as well as frequencies less than 1500 cm^{-1} comprising vibrational marker bands of photosensitizer 5CE. (inset) Magnification of the COOH regime. The band changes are specific for functional HYDA1 (black) and not observed in HYDA1 apoprotein (red). * 2337 cm^{-1}, assigned to CO_2.

changes in the OH and SH regime (Figure S4). However, the lack thereof suggests an invariable hydrogen-bonding network between the water cluster W1, C169, and the ADT headgroup of the H-cluster (Figure 1a).

Band Fitting and Tentative Assignments. The **Hred** − **Hox** spectrum in the COOH regime was described by a fit routine including a minimum of nine Gaussians with a fixed half-max width of 6−8 cm^{-1} and third-order polynomial baseline correction (Figure 3a). The temporal evolution of these bands is in excellent agreement with those of the H-

DOI: 10.1021/jacs.9b09225
J. Am. Chem. Soc. 2019, 141, 17394−17403

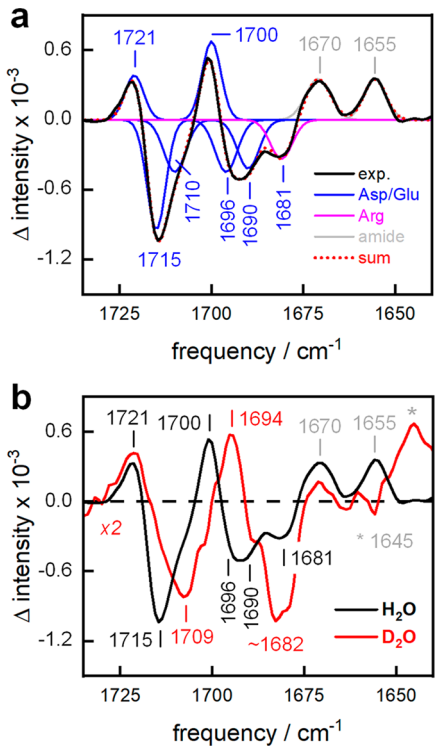

Figure 3. Band fit and H/D exchange. (a) The experimental ATR FTIR difference spectrum of the **Hred** − **Hox** conversion (black) was fitted with a minimum of six Gaussians in the COOH regime of aspartic or glutamic acid residues (blue), a single band that may stem from the $C(NH_2)_3^+$ vibration of an arginine (magenta), and two contributions in the amide regime (gray). The red dotted line depicts the resulting sum of fits. (b) Comparison of ATR FTIR difference spectra on hydrated and deuterated film (black and red, respectively). The data indicate a downshift of 6−14 cm^{-1} for bands associated with **Hox** (negative intensities) and similar frequency difference for bands accumulating upon reduction (positive intensities). No significant shift was noted for the positive bands at 1721 and ∼1670 cm^{-1}.

cluster (Figure S1). Vibrations at frequencies greater than 1700 cm^{-1} are typically assigned to the C═O stretches of the COOH side chain from aspartic acid or glutamic acid residues (E, D).[57,59] The C═O stretching frequency is inversely proportional to the hydrogen-bonding strength and can vary between none to multiple hydrogen-bonding partners from 1750 to 1700 cm^{-1}. Besides clearly discriminable bands at 1721, 1715, and 1700 cm^{-1} our fit routine suggested additional contributions centered at 1710, 1696, 1690, and 1681 (Figure 3a). The negative band at 1681 cm^{-1} may be attributed to the asymmetric $C(NH_2)_3^+$ vibration of the protonated arginine side chain,[60−62] while the broader features at ∼1670 and 1655 cm^{-1} potentially arise from changes in amide I absorbance.[63] The latter likely reflects minor changes in secondary structure induced upon reduction of the H-cluster.

H/D Exchange. To achieve an experimental band assignment in the COOH regime, we performed photoreduction on hydrated and deuterated hydrogenases films. Bands indicative of hydrogen bonding or protonation changes involving the carboxylic side chains are supposed to shift to lower frequencies in deuterated sample.[63] Absorbance spectra of the HYDA1/5CE/EDTA reaction mixture show a complete exchange of solvent in the presence of either H_2O or D_2O, and **Hred** − **Hox** difference spectra prove that deuteration did not affect the H-clusters' CO/CN^- band position (Figure S5). However, in the COOH regime, the spectra show significant changes (Figure 3b). The prominent H/D shift of 1715 and 1700 cm^{-1} to 1709 and 1694 cm^{-1} immediately supports an assignment of this motif to a titratable group, for example, an aspartic or glutamic acid side chain. Bands at 1696 and 1690 cm^{-1} were affected by the H/D shift as well. While a dissection of components is not immediately possible here, the mean frequency downshift by 12 ± 2 cm^{-1} suggests strongly hydrogen-bonded aspartic or glutamic acid side chains.[57,59] The positive band at 1721 cm^{-1} is insensitive to H/D exchange.

To achieve an unambiguous experimental band assignment, we analyzed three amino acid variants of the proton transfer pathway, namely, R148A, E144D, and S189A. The enrichment of **Hred** over **Hox** depends on functional proton transfer.[33−35] In particular, amino acid residues C169 and E141 close to the H-cluster were found to be susceptible to variations of the hydrogen-bonding network, slowly accumulating the hydride state **Hhyd** over **Hox** rather than **Hred** (Figure S6). This impedes a direct comparison, and only a limited number of variants allowed screening the hydrogen-bonding changes associated with catalytic proton transfer. An invariable hydrogen-bonding network between H-cluster and E141 is in striking agreement with the aforementioned lack of hydrogen-bonding changes around W1 and C169 (Figure S4). Relative to the H-cluster, we will refer to C169, W1, and E141 as "inner core" of the proton transfer pathway.

By contrast, Figure 4 shows **Hred** − **Hox** difference spectra of HYDA1 variants that constitute the "outer core" of the proton transfer pathway, namely, R148, E144, and S189. Site-directed mutagenesis at these positions included an exchange against alanine (A). No accumulation of **Hred** was observed upon photoreduction of E144A (Figure S6) so that the conservative variation of glutamic to aspartic acid was analyzed instead. Variants R148A, E144D, and S189A adopted **Hred** upon illumination but showed only 15−25% of the native conversion efficiency (Figure S7). For comparison with native HYDA1, difference spectra were normalized to the amplitude of the band pair at 1715 and 1700 cm^{-1} that was found to be prominently conserved in all spectra. The resulting scaling factors were in good agreement with the amplitudes observed for the CO difference bands of the conversion of **Hred** over **Hox**. Figure S6 depicts the spectral transitions over time for each variant including an evaluation of signal-to-noise in the COOH regime.

Amino Acid Variant R148A. The H_2 evolution activity of ∼50% for HYDA1 variant R148A indicates that glutamic acid E144 can partially replace R148 as proton loading site.[42] Figure 4a shows an overlay of **Hred** − **Hox** difference spectra in the COOH regime for R148A and native HYDA1 (left panel). The right panel depicts an overlay of the respective CPI crystal structures. For the sake of convenience, we will use HYDA1 numbering here. Site-directed mutagenesis resulted in spectra with missing features at 1721, 1696, or 1681 cm^{-1} (marked "X"), while the shift from 1715 to 1700 cm^{-1} and a negative band at 1690 cm^{-1} was conserved.

Above, we tentatively assigned the negative feature at 1681 cm^{-1} to the asymmetric $C(NH_2)_3^+$ vibration of an arginine residue.[60−62] The evident lack of this band in amino acid variant R148A supports this assignment. Moreover, the band at 1681 cm^{-1} shifted to 1607 cm^{-1} in deuterated sample, which is in excellent agreement to guanidine hydrochloride H/D reference spectra in Figure 5. Therefore, we conclude

DOI: 10.1021/jacs.9b09225
J. Am. Chem. Soc. 2019, 141, 17394−17403

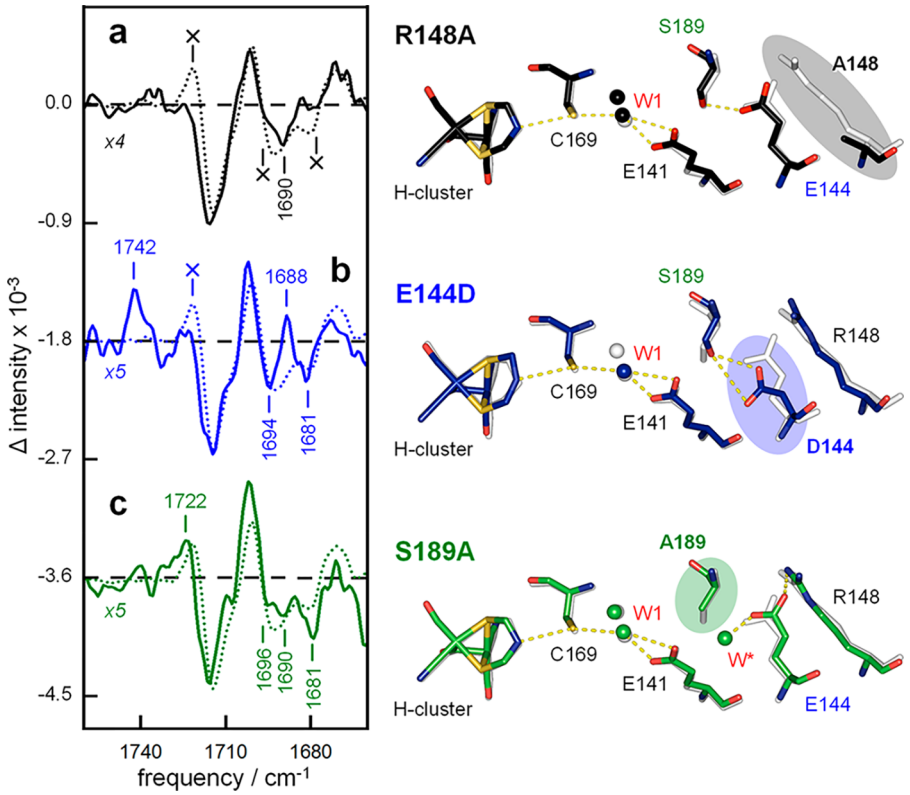

Figure 4. Spectral and structural differences between native [FeFe]-hydrogenase and three variants. (left) The *in situ* ATR FTIR difference spectra for three different amino acid variants compared to native HYDA1 (dotted traces, scaled to the 1715/1700 difference signal that was observed in all experiments). The crystallographic comparison on the right side includes CPI coordinates 4XDC, 6GM2, 6GM3, and 6GM4. (a) Arginine variant R148A lacks the positive 1721 cm^{-1} feature and shows significantly diminished contributions at 1696 and 1681 cm^{-1} ("X"). (b) Glutamic acid variant E144D exhibits an ~21 cm^{-1} upshift of the native 1721 cm^{-1} band to 1742 cm^{-1}. Negative bands at 1692 and 1682 cm^{-1} suggest similarities with native enzyme, whereas the band intensity at 1688 cm^{-1} is inverted. (c) The difference spectrum of serine variant S189A indicates a largely native behavior with only smaller differences in band intensity. See Figure S7 for further details.

deprotonation of $R148^{+}$ upon formation of **Hred** in native HYDA1. Poisson–Boltzmann calculations predicted a pK_a of ~3.5 for E144 in native HYDA1 (Table S1). Although our experiments were conducted at pH 6, we suggest hydrogen bonding of E144 to R148 (~2.8 Å) and S189 (~3.1 Å) stabilizing the carboxylic over the carboxylate form of E144. However, the carboxylate form likely prevails in the absence of the arginine side chain. The lack of spectral features at 1721 and 1696 cm^{-1} in the R148A difference spectrum (X) therefore facilitates the assignment to hydrogen-bonding changes involving E144 in native HYDA1.

Glutamic Acid Variant E144D. As observed for the arginine variant, the interaction between R148 and E144 (E144D) is not strictly essential for catalytic activity. Amino acid variant E144D is reported with ~50% H_2 evolution activity.[42] Figure 4b shows an overlay of **Hred** − **Hox** difference spectra in the COOH regime for R144D and native HYDA1 (left panel). The right panel depicts an overlay of the respective CPI crystal structures.[42] Site-directed mutagenesis resulted in spectra with a pronounced band upshift from 1721 to 1742 cm^{-1} and an intensity inversion of the band at ~1690 cm^{-1} (negative in native HYDA1, slightly shifted and positive in E144D). The band pair at 1715 and 1700 cm^{-1} and negative bands at 1694 and 1681 cm^{-1} are conserved among variant and native HYDA1.

Shortening of the alkyl side chain at position 144 causes a different hydrogen-bonding situation (Figure 4b, right panel). Instead of forming a hydrogen bond with R148 (~5.0 Å) rotation of the aspartic acid side chain forces D144 into a weak complex with S189 in **Hox** (3.0 and 3.7 Å) that reflects in a pK_a increase of nearly three units compared to native HYDA1 (Table S1). The upshift of the E144 band from 1721 to 1742 cm^{-1} suggests significantly weaker hydrogen bonding in reduced enzyme. Furthermore, variant E144D allows differentiating the 1696/1690 cm^{-1} peak doublet. The latter band appears positive in the spectrum, and thus only the 1696 cm^{-1} band is assigned to E144.

Serine Variant S189A. Figure 4c shows an overlay of **Hred** − **Hox** difference spectra in the COOH regime for S189A and native HYDA1 (left panel). The right panel depicts an overlay of the respective CPI crystal structures.[42] Despite the relatively low H_2 evolution activity of ~10%, site-directed mutagenesis resulted in spectra indicative of only minor differences to native HYDA1. The crystal structure of the S189A variant revealed an additional water molecule (W*) between E144 and E141 (Figure 4c, right panel). This arrangement was proposed to compensate the lack of the serine side chain.[42] E144 is in fair hydrogen-bonding distance to W* (~2.4 Å) and R148 (~2.9 Å), which largely restores the spectral phenotype of native HYDA1. However, the distance of 5.8 Å between E141 and W* is clearly out of range for hydrogen bonding or proton transfer.

Glutamic Acid E141. The band pair at 1715 and 1700 cm^{-1} is prominently conserved in all protein samples that accumulate **Hred** over **Hox**. The H/D specific band shift hints at a carboxylic group and suggests efficient proton exchange;

DOI: 10.1021/jacs.9b09225
J. Am. Chem. Soc. 2019, 141, 17394−17403

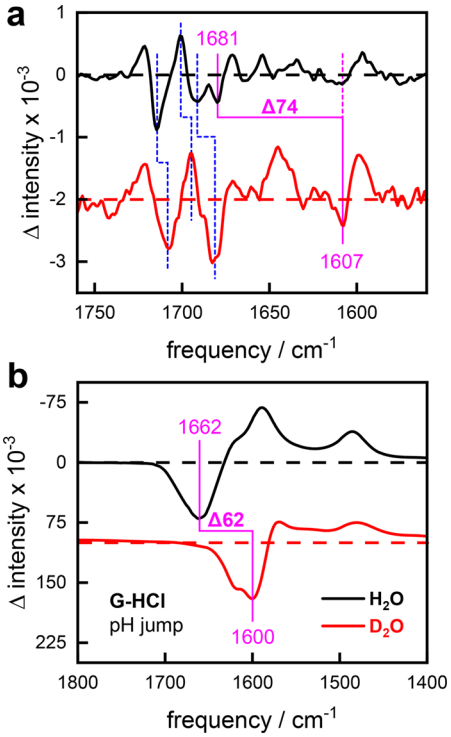

Figure 5. Experimental assignment of arginine R148. (a) Comparison of **Hred** − **Hox** difference spectra on hydrated and deuterated film (black and red, respectively) as in Figure 3. Isotope downshifts associated with COOH group are indicated by blue dashes. The band at 1681 cm^{-1} was tentatively assigned to the protonated guanidinium headgroup of $R148^+$. In the presence of D_2O, a negative feature at 1607 cm^{-1} was observed, most likely representing the deuterated arginine. (b) pH jump experiments on guanidine-HCl solved in H_2O (black) or D_2O (red). The difference spectra depict deprotonation of the guanidinium ion (negative bands) at pH ≈ 14. Both the absolute band positions and the H/D-specific downshift closely match the **Hred** − **Hox** difference spectrum in (a).

however, the motif could not be assigned to E144. Residing in a hydrophobic pocket at the interface of inner and outer core of the proton transfer pathway, glutamic acid E141 has been calculated to adopt the carboxylic acid form for pH values less than 8.[42] Accordingly, changes associated with E141 will be visible in the COOH regime.[57] Any variation of E141 abolished catalytic activity and the formation of **Hred** (Figure S5) hinting at the central role of E141 in proton transfer. On the basis of this line of evidence, we assign the band pair at 1715 and 1700 cm^{-1} to E141. Figure S7 provides a conclusive overview on the observed frequencies and experiment band assignment.

The C═O stretching frequencies of glutamic acid E141 indicate strong hydrogen-bonding contacts, irrespective of redox state.[57,59] To this end, the crystal structure of oxidized enzyme supports a *trans* complex between E141 and W1 (distances 2.4 and 3.4 Å).[64−66] The 15 cm^{-1} frequency downshift upon reduction may reflect a release of the E141/W1 complex in favor of hydrogen bonding with S189 (or W* in serine variant S189A). This demands a certain level of structural flexibility, as the distance between E141 and S189 amounts to ∼3.8 Å in oxidized enzyme. Molecular dynamics simulations showed that E141 and S189 change between hydrogen-bonding donor and acceptor when switching from proton uptake to proton release.[43,45] Apparently, smaller structural changes at the interface of inner and outer core are well within the thermodynamic range of functional [FeFe]-hydrogenases. The large distance between E141 and W* (5.8 Å) reduces the probability of proton transfer in serine variant S189A to ∼10% H_2 release activity.[42] The experimental assignment of our data is summed up in Figure 6 and Table 1.

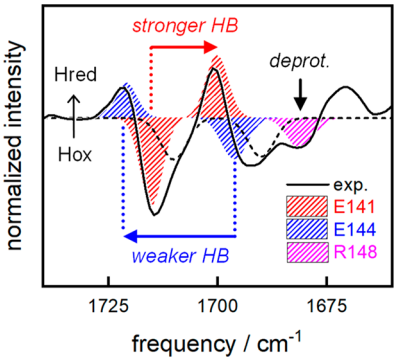

Figure 6. Band assignment. Our analysis of native [FeFe]-hydrogenase in H_2O and D_2O as well as seven different amino acid variants implies a downshift of the band at 1715 cm^{-1} by 14 cm^{-1} (red) and an upshift of the band at 1696 cm^{-1} by 25 cm^{-1} (blue). The former is assigned to E141 suggesting stronger hydrogen bonding in **Hred**. The latter is assigned to E144 suggesting the loss of a hydrogen-bonding partner (weaker hydrogen bonding). The negative band at 1681 cm^{-1} (magenta) is assigned to deprotonation of $R148^+$ upon formation of **Hred**. No conclusive assignment is available for the bands at 1710 and 1690 cm^{-1} (dashed traces).

Table 1. Band Assignment[a]

ν, cm^{-1}	redoxstate	residue	H-bonds	donor	acceptor
1742*	Hred	D144	none		
1721	Hred	E144	single	S189	
1715	Hox	E141	double	W1	
1700	Hred	E141	double	W1	S189
1696	Hox	E144	double	R148	S189
1681	Hox	$R148^+$	single		E144

[a]IR frequencies (ν) refer to native HYDA1 except as noted (*). The identity of hydrogen-bonding partners differs between amino acid variants.

DISCUSSION

Figure 7a depicts the progression of amino acid residues involved in catalytic proton transfer as identified in the crystal structure of oxidized [FeFe]-hydrogenase (**Hox**).[42] This arrangement favors proton uptake and H_2 evolution. Arginine $R148^+$ donates a hydrogen bond to glutamic acid E144 (3.1 Å), the latter forming a hydrogen bond with serine S189 (2.8 Å).[43−45] On the basis of pK_a calculations, we previously favored an ionic bond between $R148^+$ and the carboxylate of E144;[42] however, such stabilization fails to explain the FTIR band changes. Trapped between R148 and S189, E144 likely persists in protonated, carboxylic acid form, even at pH values well above the predicted pK_a of 3.5 (Table S1).

Serine S189 is located at the interface of inner and outer core of the proton transfer pathway, as defined above. The distance of ∼3.8 Å between S189 and E141 does reflect discontinued hydrogen bonding, and the probability of proton transfer appears insufficient to justify turnover frequencies greater than 10 000 H_2 s^{-1}.[9−11] The crystal structure supports

DOI: 10.1021/jacs.9b09225
J. Am. Chem. Soc. 2019, 141, 17394−17403

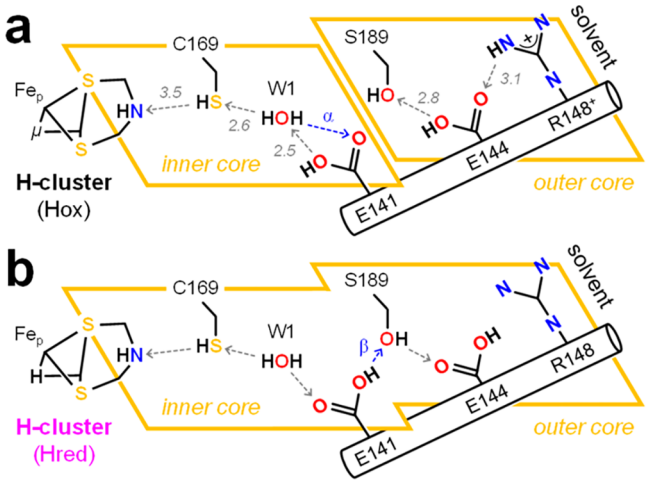

Figure 7. The hydrogen-bonding network of the catalytic proton transport pathway. (a) Progression of amino acid residues as observed in the crystal structure of oxidized [FeFe]-hydrogenase CPI (**Hox**). All distances refer to pdb coordinates 4XDC (HYDA1 numbering). Our data suggest hydrogen-bonding contacts between S189, E144, and R148$^+$ of the catalytic proton transport pathway. Furthermore, invariable hydrogen bonding between ADT, C169, and W1 was observed. The W1/E141 complex establishes the difference between inner and outer core of the catalytic proton transport pathway. (b) In reduced [FeFe]-hydrogenase (**Hred**), the W1/141 complex is terminated in favor of hydrogen bonding between E141, S189, and E144, which facilitates continuous proton transfer (see main text for details). Our data indicate deprotonation of R148$^+$ upon formation of **Hred**.

E141 and water molecule W1 forming a *trans* complex that represents the most stable configuration of COOH groups in aqueous solution.[64−66] This arrangement would interrupt the catalytic hydrogen-bonding network as indicated by the yellow boxes in Figure 7. The E141/W1 complex is weakened by the relatively long donor distance (α = 3.4 Å), which may alleviate changing from W1 to S189 as hydrogen-bond acceptor, for example, upon reduction of the H-cluster.

Our IR data are compatible with subtle structural changes upon formation of **Hred**. Figure 7b illustrates how the catalytic proton transfer pathway between active site cofactor and solvent is significantly more continuous in the reduced enzyme. The downshift of the E141 band may reflect dissolution of the E141/W1 complex and hydrogen bonding to S189 with $\alpha > \beta$ (in the oxidized crystal, β is 0.4 Å larger than α; see Figure 7a). Serine S189 donates a single bond to E144; however, no second hydrogen bond is formed by E144 due to deprotonation of R148$^+$. This is in agreement with the pronounced upshift of the E144 band. We assume that a reprotonation of R148 is precluded by the unfavorable local electrostatics betweenE144 and R148$^+$. Our data support a model in which the E144/R148 interface is defined by the OH donor group of the E144 side chain, held in place by a hydrogen bond from S189 (Figure 7b). Formation of R148$^+$ appears to be hindered in the presence of a potential hydrogen-bonding donor. The stability of deprotonated arginine residues in proteins has been questioned[67] and, to our knowledge, has not been observed before. Yet, our spectroscopic investigation on hydrated and deuterated [FeFe]-hydrogenase clearly allows concluding deprotonation of R148$^+$ upon reduction of the enzyme. This conserved arginine functions as proton donor to the active site cofactor, fine-tuning proton transfer efficiency and catalytic bias.

The mechanism of discontinuous proton transfer conceptualized above likely includes a transient step we can speculate about now. Reduction of the H-cluster by one electron leads to an increase in basicity and the formation of **Hred** upon protonation via the catalytic proton transfer pathway. On the basis of the lack of difference signals in the SH and OH regime, we consider a rigid donor/acceptor conformation between the H-cluster, C169, and W1. Protonation of the ADT headgroup in **Hred** was discussed[33−35] and computed earlier,[43−45] but the present data do not support *steady-state* protonation changes at the ADT headgroup, cysteine thiolate, or water cluster. Transiently, however, formation of **Hred** may trigger deprotonation of E141 (Figure S8). In a second step, the high basicity of E141$^-$ would induce steady-state deprotonation of R148$^+$, proton transfer via E144 and S189, and reprotonation of E141, now hydrogen-bonded to S189 instead of W1 (Figure 7b).

CONCLUSIONS

In this work, we demonstrate how *in situ* infrared spectroscopy was applied to analyze the hydrogen-bonding network of the catalytic proton transfer pathway in [FeFe]-hydrogenases. Discontinuous proton transfer was triggered by the enhanced basicity of the active site cofactor (H-cluster) upon photoreduction of a highly active iron−sulfur enzyme lacking a natural chromophore. Infrared spectroscopy provides a direct read-out for changes in hydrogen bonding perfectly complementary to X-ray crystallography. Thereby, the first experimental description of the dynamic hydrogen-bonding changes in the catalytic proton transfer pathway of [FeFe]-hydrogenases was accomplished.

Discontinuous proton transfer is common in nature, for example, in retinal proteins,[68,69] photosystem II,[70] cytochrome *c* oxidase,[71] and other systems,[48,72] but it has not yet been considered in hydrogenases. Our model rationalizes how ions transcend the gap between inner and outer core of the proton transfer pathway. Furthermore, it provides a reasonable explanation for the catalytic bidirectionality of [FeFe]-hydrogenases.[6−8] Glutamic acid E141 switches as hydrogen-bonding donor between W1 (proton uptake) and S189 (proton release). Deviations in distance less than 0.5 Å suggest a flexible hydrogen-bonding network that facilitates both H_2 evolution (proton uptake) and H_2 oxidation (proton release).

ASSOCIATED CONTENT

Supporting Information

The Supporting Information is available free of charge on the ACS Publications website at DOI: 10.1021/jacs.9b09225.

Band fitting and kinetic description; spectral characteristics of the photosensitizers; COOH band changes; spectral transitions over time; H/D exchange; accumulation of Hhyd; comparison of CO/CN and COOH difference spectra; assignment of hydrogen-bonding changes; hypothetical intermediate of proton transfer; Propka calculations (PDF)

AUTHOR INFORMATION

Corresponding Author

*sven.stripp@fu-berlin.de

DOI: 10.1021/jacs.9b09225
J. Am. Chem. Soc. 2019, 141, 17394−17403

ORCID

Jifu Duan: 0000-0002-5158-2253
Günther Knör: 0000-0002-2259-6496
Ulf-Peter Apfel: 0000-0002-1577-2420
Thomas Happe: 0000-0003-1206-5234
Joachim Heberle: 0000-0001-6321-2615
Sven Timo Stripp: 0000-0002-8412-0258

Notes

The authors declare no competing financial interest.

■ ACKNOWLEDGMENTS

We thank all reviewers for their valuable input. This project was supported by the following agencies: Deutsche Forschungsgemeinschaft (DFG) through the priority program 1927 to S.T.S. (grant 1554/5-1), the SFB 1078, and Cluster of Excellence UniSysCat to J.H. T.H., M.W., and J.D. are grateful for funding from Cluster of Excellence RESOLV (EXC2033, project 390677874), the DFG Training Group GRK 2341 Microbial Substrate Conversion (MiCon), Volkswagen Stiftung (Design of [FeS] cluster containing MetalloDNAzymes, Az 93412), and the China Scholarship Council. G.K. acknowledges funding by the Austrian Science Fund (FWF, project DK W-1250 B20).

■ REFERENCES

(1) Lubitz, W.; Ogata, H.; Rudiger, O.; Reijerse, E. Hydrogenases. *Chem. Rev.* **2014**, *114* (8), 4081−4148.

(2) Vignais, P. M.; Billoud, B. Occurrence, Classification, and Biological Function of Hydrogenases: An Overview. *Chem. Rev.* **2007**, *107* (10), 4206−4272.

(3) Thauer, R. K.; Kaster, A.-K.; Goenrich, M.; Schick, M.; Hiromoto, T.; Shima, S. Hydrogenases from Methanogenic Archaea, Nickel, a Novel Cofactor, and H2 Storage. *Annu. Rev. Biochem.* **2010**, *79*, 507−536.

(4) Fritsch, J.; Lenz, O.; Friedrich, B. Structure, Function and Biosynthesis of O2-Tolerant Hydrogenases. *Nat. Rev. Microbiol.* **2013**, *11* (2), 106−114.

(5) Peters, J. W.; Schut, G. J.; Boyd, E. S.; Mulder, D. W.; Shepard, E. M.; Broderick, J. B.; King, P. W.; Adams, M. W. [FeFe]- and [NiFe]-Hydrogenase Diversity, Mechanism, and Maturation. *Biochim. Biophys. Acta, Mol. Cell Res.* **2015**, *1853* (6), 1350−1369.

(6) Stripp, S. T.; Happe, T. How Algae Produce Hydrogen - News from the Photosynthetic Hydrogenase. *Dalt. Trans.* **2009**, *45*, 9960−9969.

(7) Wittkamp, F.; Senger, M.; Stripp, S. T.; Apfel, U.-P. [FeFe]-Hydrogenases: Recent Developments and Future Perspectives. *Chem. Commun.* **2018**, *54*, 5934−5942.

(8) Fourmond, V.; Wiedner, E. S.; Shaw, W. J.; Leger, C. On the Understanding and Design of Bidirectional and Reversible Catalysts Of. *J. Am. Chem. Soc.* **2019**, *141* (28), 11269−11285.

(9) Vincent, K. A.; Parkin, A.; Armstrong, F. A. Investigating and Exploiting the Electrocatalytic Properties of Hydrogenases. *Chem. Rev.* **2007**, *107* (10), 4366−4413.

(10) Greco, C.; Fourmond, V.; Baffert, C.; Wang, P.; Dementin, S.; Bertrand, P.; Bruschi, M.; Blumberger, J.; De Gioia, L.; Léger, C. Combining Experimental and Theoretical Methods to Learn about the Reactivity of Gas-Processing Metalloenzymes. *Energy Environ. Sci.* **2014**, *7*, 3543−3573.

(11) Armstrong, F. A.; Evans, R. M.; Hexter, S. V.; Murphy, B. J.; Roessler, M. M.; Wulff, P. Guiding Principles of Hydrogenase Catalysis Instigated and Clarified by Protein Film Electrochemistry. *Acc. Chem. Res.* **2016**, *49* (5), 884−892.

(12) Barton, B. E.; Olsen, M. T.; Rauchfuss, T. B. Artificial Hydrogenases. *Curr. Opin. Biotechnol.* **2010**, *21* (3), 292−297.

(13) Simmons, T. R.; Berggren, G.; Bacchi, M.; Fontecave, M.; Artero, V. Mimicking Hydrogenases: From Biomimetics to Artificial Enzymes. *Coord. Chem. Rev.* **2014**, *270*−*271* (1), 127−150.

(14) Möller, F.; Piontek, S.; Miller, R. G.; Apfel, U.-P. From Enzymes To Functional Materials - Towards Activation Of Small Molecules. *Chem. - Eur. J.* **2018**, *24* (7), 1471−1493.

(15) Peters, J. W.; Lanzilotta, W. N.; Lemon, B. J.; Seefeldt, L. C. X-Ray Crystal Structure of the Fe-Only Hydrogenase (CpI) from Clostridium Pasteurianum to 1.8 Angstrom Resolution. *Science* **1998**, *282* (5395), 1853−1858.

(16) Nicolet, Y.; Piras, C.; Legrand, P.; Hatchikian, C. E.; Fontecilla-Camps, J. C. Desulfovibrio Desulfuricans Iron Hydrogenase: The Structure Shows Unusual Coordination to an Active Site Fe Binuclear Center. *Structure* **1999**, *7* (1), 13−23.

(17) Esselborn, J.; Muraki, N.; Klein, K.; Engelbrecht, V.; Metzler-Nolte, N.; Apfel, U.-P.; Hofmann, E.; Kurisu, G.; Happe, T. A Structural View of Synthetic Cofactor Integration into [FeFe]-Hydrogenases. *Chem. Sci.* **2016**, *7*, 959−968.

(18) Pierik, A. J.; Hulstein, M.; Hagen, W. R.; Albracht, S. P. A Low-Spin Iron with CN and CO as Intrinsic Ligands Forms the Core of the Active Site in [Fe]-Hydrogenases. *Eur. J. Biochem.* **1998**, *258* (2), 572−578.

(19) De Lacey, A. L.; Stadler, C.; Cavazza, C.; Hatchikian, E. C.; Fernandez, V. M. FTIR Characterization of the Active Site of the Fe-Hydrogenase from Desulfovibrio Desulfuricans. *J. Am. Chem. Soc.* **2000**, *122* (45), 11232−11233.

(20) Nicolet, Y.; De Lacey, A. L.; Vernède, X.; Fernandez, V. M.; Hatchikian, E. C.; Fontecilla-Camps, J. C. Crystallographic and FTIR Spectroscopic Evidence of Changes in Fe Coordination upon Reduction of the Active Site of the Fe-Only Hydrogenase from Desulfovibrio Desulfuricans. *J. Am. Chem. Soc.* **2001**, *123* (8), 1596−1601.

(21) Silakov, A.; Wenk, B.; Reijerse, E.; Lubitz, W. 14N HYSCORE Investigation of the H-Cluster of [FeFe] Hydrogenase: Evidence for a Nitrogen in the Dithiol Bridge. *Phys. Chem. Chem. Phys.* **2009**, *11* (31), 6592.

(22) Duan, J.; Mebs, S.; Laun, K.; Wittkamp, F.; Heberle, J.; Hofmann, E.; Apfel, U.-P.; Winkler, M.; Senger, M.; Haumann, M.; Stripp, S. T.; et al. Geometry of the Catalytic Active Site in [FeFe]-Hydrogenase Is Determined by Hydrogen Bonding and Proton Transfer. *ACS Catal.* **2019**, *9*, 9140−9149.

(23) Albracht, S. P. J.; Roseboom, W.; Hatchikian, E. C. The Active Site of the [FeFe]-Hydrogenase from Desulfovibrio Desulfuricans. I. Light Sensitivity and Magnetic Hyperfine Interactions as Observed by Electron Paramagnetic Resonance. *JBIC, J. Biol. Inorg. Chem.* **2006**, *11* (1), 88−101.

(24) Roseboom, W.; De Lacey, A. L.; Fernandez, V. M.; Hatchikian, E. C.; Albracht, S. P. J. The Active Site of the [FeFe]-Hydrogenase from Desulfovibrio Desulfuricans. II. Redox Properties, Light Sensitivity and CO-Ligand Exchange as Observed by Infrared Spectroscopy. *JBIC, J. Biol. Inorg. Chem.* **2006**, *11* (1), 102−118.

(25) Silakov, A.; Reijerse, E. J.; Albracht, S. P. J.; Hatchikian, E. C.; Lubitz, W. The Electronic Structure of the H-Cluster in the [FeFe]-Hydrogenase from Desulfovibrio Desulfuricans: A Q-Band 57Fe-ENDOR and HYSCORE Study. *J. Am. Chem. Soc.* **2007**, *129* (37), 11447−11458.

(26) Katz, S.; Noth, J.; Horch, M.; Shafaat, H. S.; Happe, T.; Hildebrandt, P.; Zebger, I. Vibrational Spectroscopy Reveals the Initial Steps of Biological Hydrogen Evolution. *Chem. Sci.* **2016**, *7*, 6746−6752.

(27) Senger, M.; Mebs, S.; Duan, J.; Shulenina, O.; Laun, K.; Kertess, L.; Wittkamp, F.; Apfel, U.-P.; Happe, T.; Winkler, M.; Haumann, M.; Stripp, S. T. Protonation/Reduction Dynamics at the [4Fe−4S] Cluster of the Hydrogen-Forming Cofactor in [FeFe]-Hydrogenases. *Phys. Chem. Chem. Phys.* **2018**, *20*, 3128−3140.

(28) Mulder, D. W.; Ratzloff, M. W.; Bruschi, M.; Greco, C.; Koonce, E.; Peters, J. W.; King, P. W. Investigations on the Role of Proton-Coupled Electron Transfer in Hydrogen Activation by

DOI: 10.1021/jacs.9b09225
J. Am. Chem. Soc. 2019, 141, 17394−17403

[FeFe]-Hydrogenase. *J. Am. Chem. Soc.* **2014**, *136* (43), 15394−15402.
(29) Mulder, D. W.; Guo, Y.; Ratzloff, M. W.; King, P. W. Identification of a Catalytic Iron-Hydride at the H-Cluster of [FeFe]-Hydrogenase. *J. Am. Chem. Soc.* **2017**, *139* (1), 83−86.
(30) Winkler, M.; Senger, M.; Duan, J.; Esselborn, J.; Wittkamp, F.; Hofmann, E.; Apfel, U.-P.; Stripp, S. T.; Happe, T. Accumulating the Hydride State in the Catalytic Cycle of [FeFe]-Hydrogenases. *Nat. Commun.* **2017**, *8* (16115), 1−7.
(31) Reijerse, E. J.; Pham, C. C.; Pelmenschikov, V.; Gilbert-Wilson, R.; Adamska-Venkatesh, A.; Siebel, J. F.; Gee, L. B.; Yoda, Y.; Tamasaku, K.; Lubitz, W.; Rauchfuss, T. B.; Cramer, S. P. Direct Observation of an Iron-Bound Terminal Hydride in [FeFe]-Hydrogenase by Nuclear Resonance Vibrational Spectroscopy. *J. Am. Chem. Soc.* **2017**, *139* (12), 4306−4309.
(32) Senger, M.; Laun, K.; Wittkamp, F.; Duan, J.; Haumann, M.; Happe, T.; Winkler, M.; Apfel, U.-P.; Stripp, S. T. Proton-Coupled Reduction of the Catalytic [4Fe-4S] Cluster in [FeFe]-Hydrogenases. *Angew. Chem., Int. Ed.* **2017**, *56* (52), 16503−16506.
(33) Adamska-Venkatesh, A.; Silakov, A.; Lambertz, C.; Rüdiger, O.; Happe, T.; Reijerse, E.; Lubitz, W. Identification and Characterization of the "Super-Reduced" State of the H-Cluster in [FeFe] Hydrogenase: A New Building Block for the Catalytic Cycle? *Angew. Chem., Int. Ed.* **2012**, *51* (46), 11458−11462.
(34) Sommer, C.; Adamska-Venkatesh, A.; Pawlak, K.; Birrell, J. A.; Rüdiger, O.; Reijerse, E. J.; Lubitz, W. Proton Coupled Electronic Rearrangement within the H-Cluster as an Essential Step in the Catalytic Cycle of [FeFe] Hydrogenases. *J. Am. Chem. Soc.* **2017**, *139* (4), 1440−1443.
(35) Mebs, S.; Senger, M.; Duan, J.; Wittkamp, F.; Apfel, U.-P.; Happe, T.; Winkler, M.; Stripp, S. T.; Haumann, M. Bridging Hydride at Reduced H-Cluster Species in [FeFe]-Hydrogenases Revealed by Infrared Spectroscopy, Isotope Editing, and Quantum Chemistry. *J. Am. Chem. Soc.* **2017**, *139* (35), 12157−12160.
(36) Haumann, M.; Stripp, S. T. The Molecular Proceedings of Biological Hydrogen Turnover. *Acc. Chem. Res.* **2018**, *51* (8), 1755−1763.
(37) Ratzloff, M. W.; Artz, J. H.; Mulder, D. W.; Collins, R. T.; Furtak, T. E.; King, P. W. CO-Bridged H-Cluster Intermediates in the Catalytic Mechanism of [FeFe]-Hydrogenase CaI. *J. Am. Chem. Soc.* **2018**, *140* (24), 7623−7628.
(38) Fourmond, V.; Greco, C.; Sybirna, K.; Baffert, C.; Wang, P.-H.; Ezanno, P.; Montefiori, M.; Bruschi, M.; Meynial-Salles, I.; Soucaille, P.; Blumberger, J.; Bottin, H.; De Gioia, L.; Léger, C. The Oxidative Inactivation of FeFe Hydrogenase Reveals the Flexibility of the H-Cluster. *Nat. Chem.* **2014**, *6* (4), 336−342.
(39) Cornish, A. J.; Gärtner, K.; Yang, H.; Peters, J. W.; Hegg, E. L. Mechanism of Proton Transfer in [FeFe]-Hydrogenase from Clostridium Pasteurianum. *J. Biol. Chem.* **2011**, *286*, 38341−38347.
(40) Morra, S.; Giraudo, A.; Di Nardo, G.; King, P. W.; Gilardi, G.; Valetti, F. Site Saturation Mutagenesis Demonstrates a Central Role for Cysteine 298 as Proton Donor to the Catalytic Site in CaHydA [FeFe]-Hydrogenase. *PLoS One* **2012**, *7* (10), No. e48400.
(41) Cornish, A. J.; Ginovska, B.; Thelen, A.; Da Silva, J. C. S.; Soares, T. A.; Raugei, S.; Dupuis, M.; Shaw, W. J.; Hegg, E. L. Single-Amino Acid Modifications Reveal Additional Controls on the Proton Pathway of [FeFe]-Hydrogenase. *Biochemistry* **2016**, *55* (22), 3165−3173.
(42) Duan, J.; Senger, M.; Esselborn, J.; Engelbrecht, V.; Wittkamp, F.; Apfel, U.-P.; Hofmann, E.; Stripp, S. T.; Happe, T.; Winkler, M. Crystallographic and Spectroscopic Assignment of the Proton Transfer Pathway in [FeFe]-Hydrogenases. *Nat. Commun.* **2018**, *9*, 4726.
(43) Long, H.; King, P. W.; Chang, C. H. Proton Transport in Clostridium Pasteurianum [FeFe] Hydrogenase I: A Computational Study. *J. Phys. Chem. B* **2014**, *118* (4), 890−900.
(44) Sode, O.; Voth, G. a. Electron Transfer Activation of a Second Water Channel for Proton Transport in [FeFe]-Hydrogenase. *J. Chem. Phys.* **2014**, *141* (22), 22D527.
(45) Ginovska-Pangovska, B.; Ho, M.-H.; Linehan, J. C.; Cheng, Y.; Dupuis, M.; Raugei, S.; Shaw, W. J. Molecular Dynamics Study of the Proposed Proton Transport Pathways in [FeFe]-Hydrogenase. *Biochim. Biophys. Acta, Bioenerg.* **2014**, *1837* (1), 131−138.
(46) Garczarek, F.; Gerwert, K. Functional Waters in Intraprotein Proton Transfer Monitored by FTIR Difference Spectroscopy. *Nature* **2006**, *439*, 216−219.
(47) Debus, R. J. FTIR Studies of Metal Ligands, Networks of Hydrogen Bonds, and Water Molecules near the Active Site Mn4CaO5 Cluster in Photosystem II. *Biochim. Biophys. Acta, Bioenerg.* **2015**, *1847* (1), 19−34.
(48) Kottke, T.; Lórenz-Fonfría, V. A.; Heberle, J. The Grateful Infrared: Sequential Protein Structural Changes Resolved by Infrared Difference Spectroscopy. *J. Phys. Chem. B* **2017**, *121*, 335−350.
(49) Lübben, M.; Gerwert, K. Redox FTIR Difference Spectroscopy Using Caged Electrons Reveals Contributions of Carboxyl Groups to the Catalytic Mechanism of Haem-Copper Oxidases. *FEBS Lett.* **1996**, *397* (2−3), 303−307.
(50) Adam, D.; Bösche, L.; Castaneda-Losada, L.; Winkler, M.; Apfel, U.-P.; Happe, T. Sunlight-Dependent Hydrogen Production by Photosensitizer/Hydrogenase Systems. *ChemSusChem* **2017**, *10*, 894−902.
(51) Esselborn, J.; Lambertz, C.; Adamska-Venkatesh, A.; Simmons, T.; Berggren, G.; Noth, J.; Siebel, J. F.; Hemschemeier, A.; Artero, V.; Reijerse, E.; Fontecave, M.; Lubitz, W.; Happe, T. Spontaneous Activation of [FeFe]-Hydrogenases by an Inorganic [2Fe] Active Site Mimic. *Nat. Chem. Biol.* **2013**, *9*, 607−609.
(52) Berggren, G.; Adamska-Venkatesh, A.; Lambertz, C.; Simmons, T. R.; Esselborn, J.; Atta, M.; Gambarelli, S.; Mouesca, J.-M.; Reijerse, E. J.; Lubitz, W.; Happe, T.; Artero, V.; Fontecave, M. Biomimetic Assembly and Activation of [FeFe]-Hydrogenases. *Nature* **2013**, *499* (7456), 66−69.
(53) Senger, M.; Mebs, S.; Duan, J.; Wittkamp, F.; Apfel, U.-P.; Heberle, J.; Haumann, M.; Stripp, S. T. Stepwise Isotope Editing of [FeFe]-Hydrogenases Exposes Cofactor Dynamics. *Proc. Natl. Acad. Sci. U. S. A.* **2016**, *113* (30), 8454−8459.
(54) Knör, G. The Concept of Photochemical Enzyme Models − State of the Art. *Coord. Chem. Rev.* **2016**, *325*, 102−115.
(55) Kandori, H. Role of Internal Water Molecules in Bacteriorhodopsin. *Biochim. Biophys. Acta, Bioenerg.* **2000**, *1460* (1), 177−191.
(56) Lórenz-Fonfría, V. A.; Muders, V.; Schlesinger, R.; Heberle, J. Changes in the Hydrogen-Bonding Strength of Internal Water Molecules and Cysteine Residues in the Conductive State of Channelrhodopsin-1. *J. Chem. Phys.* **2014**, *141* (22), 22D507.
(57) Barth, A. The Infrared Absorption of Amino Acid Side Chains. *Prog. Biophys. Mol. Biol.* **2000**, *74* (3−5), 141−173.
(58) Tai, H.; Nishikawa, K.; Higuchi, Y.; Mao, Z.-W.; Hirota, S. Cysteine SH and Glutamate COOH Contributions to [NiFe] Hydrogenase Proton Transfer Revealed by Highly Sensitive FT-IR Spectroscopy. *Angew. Chem., Int. Ed.* **2019**, *58* (38), 13285−13290.
(59) Nie, B.; Stutzman, J.; Xie, A. A Vibrational Spectral Maker for Probing the Hydrogen-Bonding Status of Protonated Asp and Glu Residues. *Biophys. J.* **2005**, *88* (4), 2833−2847.
(60) Jones, W. J. The Infra-Red Spectrum and Structure of Guanidine. *Trans. Faraday Soc.* **1959**, *55*, 524−527.
(61) Venyaminov, S. Y.; Kalnin, N. N. Quantitative IR Spectrophotometry of Peptide Compounds in Water (H2O) Solutions. I. Spectral Parameters of Amino Acid Residue Absorption Bands. *Biopolymers* **1990**, *30* (13−14), 1243−1257.
(62) Braiman, M. S.; Briercheck, D. M.; Kriger, K. M. Modeling Vibrational Spectra of Amino Acid Side Chains in Proteins: Effects of Protonation State, Counterion, and Solvent on Arginine C-N Stretch Frequencies †. *J. Phys. Chem. B* **1999**, *103* (22), 4744−4750.
(63) Barth, A. Infrared Spectroscopy of Proteins. *Biochim. Biophys. Acta, Bioenerg.* **2007**, *1767* (9), 1073−1101.
(64) Priem, D.; Ha, T. K.; Bauder, A. Rotational Spectra and Structures of Three Hydrogen-Bonded Complexes between Formic Acid and Water. *J. Chem. Phys.* **2000**, *113* (1), 169−175.

DOI: 10.1021/jacs.9b09225
J. Am. Chem. Soc. 2019, 141, 17394−17403

(65) Aloisio, S.; Hintze, P. E.; Vaida, V. The Hydration of Formic Acid. *J. Phys. Chem. A* **2002**, *106* (2), 363−370.
(66) Müller-Dethlefs, K.; Hobza, P. Noncovalent Interactions: A Challenge for Experiment and Theory. *Chem. Rev.* **2000**, *100* (1), 143−168.
(67) Harms, M. J.; Schlessman, J. L.; Sue, G. R.; Garcia-Moreno, B. Arginine Residues at Internal Positions in a Protein Are Always Charged. *Proc. Natl. Acad. Sci. U. S. A.* **2011**, *108* (47), 18954−18959.
(68) Lorenz-Fonfria, V. A.; Resler, T.; Krause, N.; Nack, M.; Gossing, M.; Fischer von Mollard, G.; Bamann, C.; Bamberg, E.; Schlesinger, R.; Heberle, J. Transient Protonation Changes in Channelrhodopsin-2 and Their Relevance to Channel Gating. *Proc. Natl. Acad. Sci. U. S. A.* **2013**, *110* (14), E1273−E1281.
(69) Lorenz-Fonfria, V. A.; Saita, M.; Lazarova, T.; Schlesinger, R.; Heberle, J. PH-Sensitive Vibrational Probe Reveals a Cytoplasmic Protonated Cluster in Bacteriorhodopsin. *Proc. Natl. Acad. Sci. U. S. A.* **2017**, *114* (51), E10909−E10918.
(70) McEvoy, J. P.; Brudvig, G. W. Water-Splitting Chemistry of Photosystem II. *Chem. Rev.* **2006**, *106* (11), 4455−4483.
(71) Nyquist, R. M.; Heitbrink, D.; Bolwien, C.; Gennis, R. B.; Heberle, J. Direct Observation of Protonation Reactions during the Catalytic Cycle of Cytochrome c Oxidase. *Proc. Natl. Acad. Sci. U. S. A.* **2003**, *100* (15), 8715−8720.
(72) Ishikita, H.; Saito, K. Proton Transfer Reactions and Hydrogen-Bond Networks in Protein Environments. *J. R. Soc., Interface* **2014**, *11* (91), 20130518.

DOI: 10.1021/jacs.9b09225
J. Am. Chem. Soc. 2019, 141, 17394−17403